THE JOURNAL OF PHYSICAL CHEMISTRY B

Article

pubs.acs.org/JPCB

X-ray Diffraction and Vibrational Spectroscopic Study of the Influence of Cis- and Trans-Unsaturation on the α-Phase of Triacylglycerols

Chikayo Takechi[†,‡] and Fumitoshi Kaneko*[,†]

[†]Department of Macromolecular Science, Graduate School of Science, Osaka University, Toyonaka, Osaka 560-0043, Japan

[‡]Department of Chemical Science and Engineering, Graduate School of Engineering, Kobe University, Rokko, Nada, Kobe 657-8501, Japan

ABSTRACT: In order to clarify how cis- and trans-unsaturation of acyl chains influences the structure and properties of the metastable α-phase of triacylglycerols (TAGs), the conformation and packing of acyl chains and their temperature dependence were investigated by means of vibrational spectroscopy (IR and Raman) and powder X-ray diffractometry for typical saturated and cis- and trans-unsaturated TAGs, namely, tristearin, triolein, and trielaidin, which have clarified the following characteristics of each TAG. In the high-temperature range close to the melting point, the acyl chains form the hexagonal subcell for tristearin and trielaidin but they build the pseudohexagonal subcell for triolein. On the other hand, both cis- and trans-double bonds have a significant influence on the conformation of acyl chains. In triolein and trielaidin where the acyl chains are divided into two parts by a C=C bond, namely, the methyl-sided and the glycerol-sided chains, the glycerol-sided chain exhibits selective conformational disordering in the α-phase of these TAGs. The structural changes of acyl chains caused by cooling are also significantly affected by cis- and trans-unsaturation. For tristearin, the greater part of hydrocarbon segments change their packing from the hexagonal subcell to the pseudohexagonal subcell by cooling, while the greater part of hydrocarbon segments keep the hexagonal subcell structure and only the smaller part of them transform to the pseudohexagonal subcell for trielaidin. On the other hand, triolein does not exhibit any major changes with respect to subcell structure on cooling.

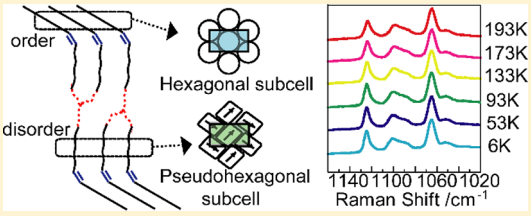

INTRODUCTION

Polymorphism is one of the important properties of triacylglycerols (TAGs) from scientific and practical points of view. Depending on crystallization conditions, subsequent heat treatments, and fatty acid constituent, a few or more crystalline states are generated. Among a variety of solid states of TAGs, the structure of the stable phase β has been studied most eagerly and extensively.[1−7] Compared with the β-phase, structural information about the metastable phases is scarce except for a few reports about the crystal structure of the β'-phase.[8−10] However, most TAGs used as ingredients for various industrial products are in a condition of metastable phase. Such metastable phases are industrially more important than the β-phase. For example, TAGs are found as α or β' or their mixture in ice cream and as β' in margarine and shortening.[11−15]

Therefore, knowledge about the structures of the metastable phases at a molecular level is of fundamental importance for understanding the physical properties of lipid compounds and designing a product containing fats and lipids. Although the acyl chain composition has a significant influence on the polymorphism of TAGs, the relation of acyl chain composition to the structure of the metastable phases has not been fully explored yet.

Unsaturation is one of the most influential factors for the solid-state structures of fats and lipids. As the first step to obtain the concrete information how unsaturation affects the structure of the metastable states, we studied the polymorphism of triolein, a representative cis-unsaturated monoacid TAG by means of powder X-ray diffraction (PXD) and vibrational spectroscopy, which showed that the cis-C=C bond in oleoyl group affects significantly the conformation and lateral packing of hydrocarbon segments in the α-phase of triolein.[16] It was also shown that in the process of cooling the α-phase of triolein exhibits rather different behavior from that of saturated TAGs.

As for TAGs and diacylglycerols with saturated acyl chains, it has been confirmed that the hexagonal (H) subcell of the α-phase transforms to another subcell reversibly on cooling.[17−23] The subcell was characterized as a pseudohexagonal (p-H) one by X-ray diffraction and IR spectroscopy, in which hydrocarbon chains are packed in an $O_{\perp}$-like subcell. This solid state obtained by cooling was named sub-α. On the other hand, information about structural changes of unsaturated TAGs on cooling is scarce.[7,16]

More elaborate studies are necessary to confirm the results of previous studies and obtain further information about the influence of cis- and trans-unsaturation on the structure and properties of the α- and sub-α-phases. In this study, we tried to disclose the characteristics of cis-unsaturation by investigating

Received: April 6, 2013
Revised: July 2, 2013
Published: July 3, 2013

the temperature-dependent structural change in detail with quantitative analysis of PXD and IR and Raman spectroscopic data and by comparing the experimental results among three representative monoacid TAGs, triolein, tristearin, and trielaidin, having respectively cis-unsaturated, saturated, and trans-unsaturated acyl chains, all with 18 carbon atoms.

We focused in particular on the lateral packing and conformation of acyl chains. The information about the lateral packing has been obtained by analyzing PXD profile in the region of spacing = 3.5−5.0 Å and infrared CH_2 rocking r(CH_2), and CH_2 scissoring δ(CH_2) region. As for the conformation, we employed Raman spectroscopy, which can probe the methyl-sided and glycerol-sided hydrocarbon chains in elaidoyl and oleoyl groups separately. By combining these two kinds of structural information, the similarities and differences between cis- and trans-unsaturation with respect to the influence on the metastable solid states of TAGs have been elucidated.

In this paper, we will concretely describe the strong impact of cis-unsaturation on the structure of the α-phase in the following way. First, we show that, with respect to the lateral packing and its temperature dependence, triolein exhibits significant difference from tristearin and trielaidin. Next, it is shown that cis- and trans-unsaturation causes selective conformational disordering in the acyl chains. The influence on the size of domain that the acyl chains form is also illustrated. Finally, we discuss the influence of cis- and trans-unsaturation on the structure of the α-phase.

EXPERIMENTAL SECTION

Samples. Tristearin, trielaidin, and triolein (>99% purity) were purchased from Sigma Co. Ltd. and used without further purification. From now on, these TAGs are denoted for short by SSS, EEE, and OOO, respectively, for which chemical structures are shown in Figure 1. The relative thermodynamic stabilities of solid modifications for these TAGs are schematically represented in Figure 2.[24] The α-phase was prepared by cooling a melt at a rate of about 10 °C/min. For IR measurements, the α-phase was grown between a couple of KBr windows.

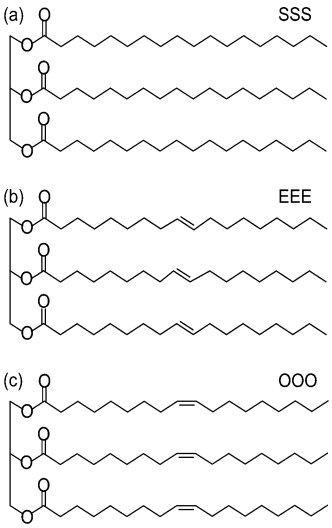

Figure 1. Chemical structures of (a) tristearin (SSS), (b) trielaidin (EEE), and (c) triolein (OOO).

Methods. PXD data were taken over 2θ range from 2 to 70° at 0.5°/min with a step size of 0.05° by using a RIGAKU RINT 2000 diffractometer with Cu Kα radiation (40 kV and 40 mA), equipped with liquid N_2 flow type cryostat for low-temperature measurements.

IR spectra were taken with a JASCO FT-IR 8300 spectrometer. The resolution and number of scans were set at 2 cm^{-1} and 64, respectively. Raman spectra were measured with a Jasco NR-1800 double monochromator using 514.5 nm line (Ar^+ laser) as an excitation source at a resolution of 3 cm^{-1}. For measurements for IR and Raman spectra at low temperatures, an Oxford liquid He flow type cryostat was employed. In order to correct the influence of temperature change on the optical conditions for Raman measurements, the scattering intensity of CH_2 twisting band at 1295 cm^{-1} was used as internal standard.[25]

Curve-fitting analyses of IR and PXD data were carried out with a software (Spectra Manager) of Jasco Co. The assignments of X-ray reflections due to subcell structures were carried out referring to the crystallographic data and indexing concerning the H and p-H subcells in the previous studies.[17,18,20−23] As for the curve-fitting analysis of PXD data, the initial values were set using the assignments and considering the influence of the thermal contraction of subcells by cooling and the contribution of other components to the background. A linear background approximation was assumed and the mixing ratio of Gaussian to Lorentzian character was treated as a variable in the iteration process. PXD data were corrected for the polarization and Lorentz factor before the curve-fitting procedures.

The weight fractions of the acyl chains adopting the H and p-H subcells,[17−23] x_H and $x_{p\text{-}H}$, were estimated from the PXD intensity data by using the following relations

$$x_H\ (\%) = \frac{I_H}{I_H + I_{p\text{-}H}} \times 100$$

and

$$x_{p\text{-}H}\ (\%) = \frac{I_{p\text{-}H}}{I_H + I_{p\text{-}H}} \times 100$$

where I_H is the integrated intensity of the reflection due to the {100} planes of the H subcell and $I_{p\text{-}H}$ is the total intensity of the two reflections due to the {110} and {200} planes due to the p-H subcell.

Similarly, x_H and $x_{p\text{-}H}$ were estimated also from the absorption intensity fraction of each subcell component in the r(CH_2) and δ(CH_2) regions.

The cross-sectional areas per chain for the H and p-H subcells, A_H and $A_{p\text{-}H}$, were estimated from the lattice spacings of subcell reflections by using the following equations

$$A_H = \frac{2}{\sqrt{3}} \times {d_{100}}^2$$

and

$$A_{p\text{-}H} = \frac{2 \times {d_{200}}^2 \times d_{110}}{\sqrt{4 \times {d_{200}}^2 - {d_{110}}^2}}$$

where d_{100} is the lattice spacing of the 100 reflection of the H subcell and d_{200} and d_{110} are the lattice spacings of the 200 and 110 reflections of the p-H subcell.

dx.doi.org/10.1021/jp4034062 | J. Phys. Chem. B 2013, 117, 8896−8905

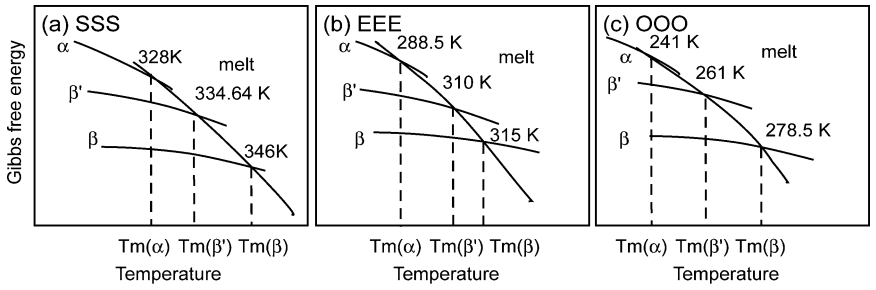

Figure 2. Relationships between the Gibbs free energy and temperature for the α, β', and β modifications of (a) SSS, (b) EEE, and (c) OOO.

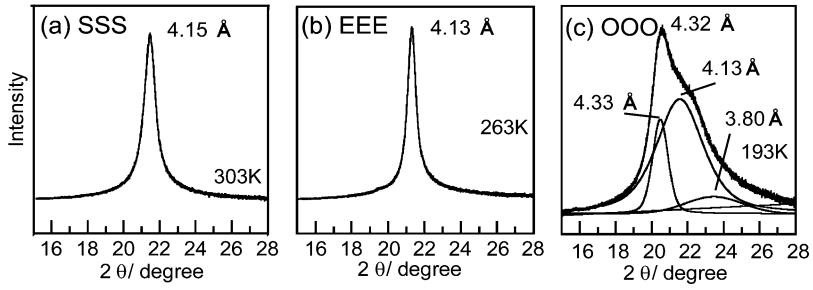

Figure 3. PXD diagrams of (a) SSS, (b) EEE, and (c) OOO. The result of the peak resolution analysis is shown in (c).

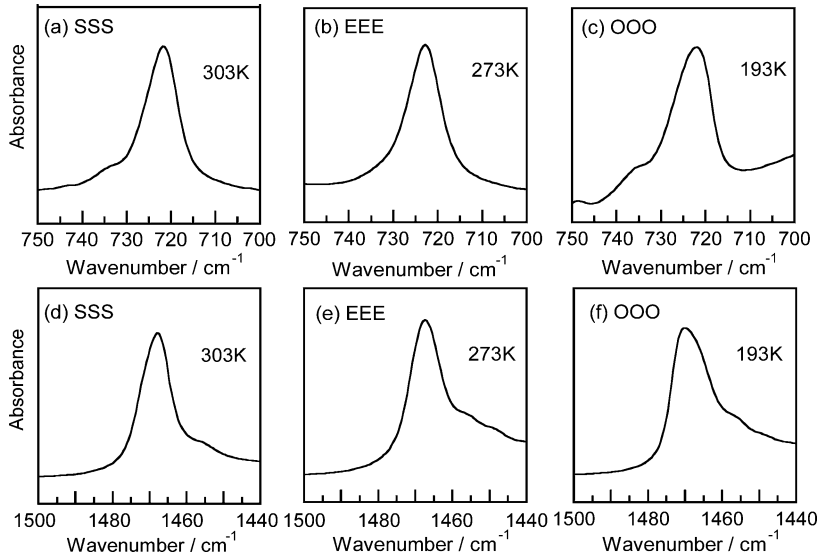

Figure 4. IR spectra in r(CH_2) (a–c) and δ(CH_2) (d–f) regions. The high background level on the low-frequency side in (c) is attributed to the foot of the intense C–H out-of-plane band due to cis-olefin group.

To evaluate the crystal domain size from the integral breadth of the PXD profile, the line broadening due to the experimental condition was corrected using the convenient method for deconvolution developed by Hindeleh and Johnson,[26] which was originally reported by Jones.[27] Assuming that the crystallite size practically dominates the peak profile after the correction of Lorentz and polarization factors, the crystallite size in the direction perpendicular to the reflecting plane, L, is estimated by using Scherrer equation

$$L = \frac{K\lambda}{\beta \cos\theta}$$

where Sherrere constant K is assumed to be 1, λ is the wavelength, θ is the Bragg angle of the diffraction peak, and β is the integral breadth in radians given by

$$\beta = \frac{\int I_b \, db}{I_{max}}$$

where b is the reciprocal space vector ($b = 2 \sin\theta/\lambda$) and the denominator and numerator mean the maximum and integrated intensity of the corresponding Bragg reflection, respectively. The influence of the distortion of the second kind was not considered in this analysis.[28−30]

RESULTS AND DISCUSSION

Lateral Packing of Acyl Chains in the α-Phase. Figure 3 shows the PXD diagram of the α-phase of OOO, in comparison with that of SSS and EEE, taken at a temperature near the melting point (OOO, 193 K; SSS, 303 K; EEE, 263 K) where the α-phase can be barely preserved during the PXD

dx.doi.org/10.1021/jp4034062 | J. Phys. Chem. B 2013, 117, 8896−8905

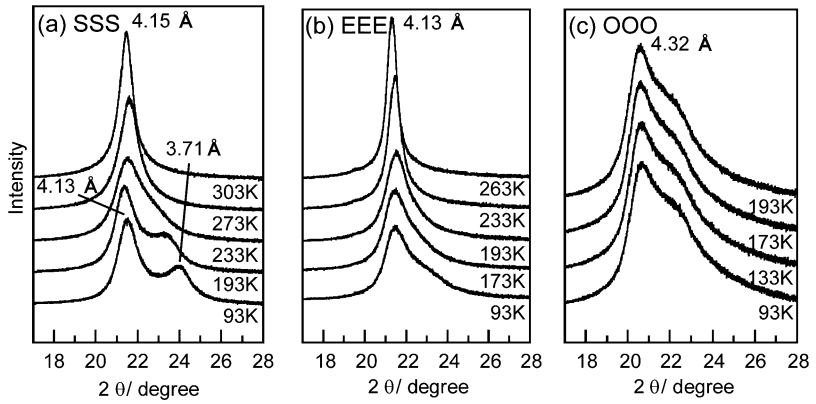

Figure 5. Temperature dependence of PXD diagrams, (a) SSS, (b) EEE, and (c) OOO.

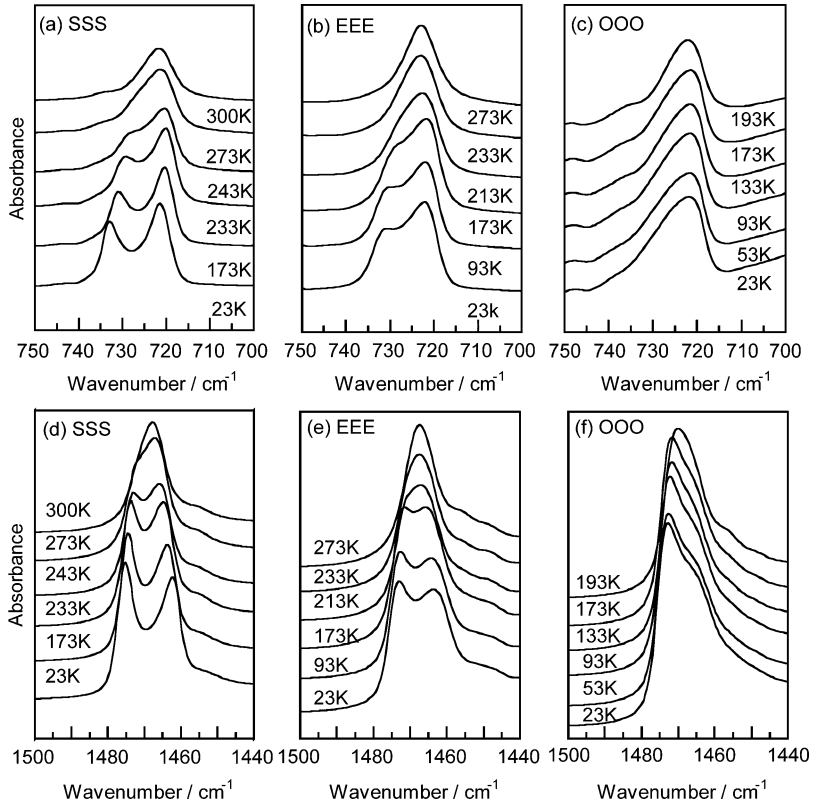

Figure 6. Temperature dependence of IR spectra in r(CH_2) (a–c) and δ(CH_2) (d–f) regions.

measurements. OOO shows a peculiar profile in the region of 2θ = 18–25° (d = 3.5–5.0 Å) sensitive to the lateral packing of hydrocarbon chains. SSS and EEE show a strong symmetric reflection due to the {100} plane of the H subcell at 2θ = 21.4° (d = 4.15 Å) and 21.5° (d = 4.13 Å), respectively. On the contrary, OOO shows a rather broadened asymmetric reflection at 20.6° (d = 4.32 Å) with a shoulder on the high angle side, indicating a rather distorted structure from the ordinary H subcell. A similar phenomenon is observed in the IR spectra. Figure 4 shows the IR spectra in the r(CH_2) and δ(CH_2) regions sensitive to the subcell structure. Compared with SSS and EEE, OOO exhibits rather asymmetrically broadened r(CH_2) and δ(CH_2) bands. The r(CH_2) band is broadened to the high-frequency side, while the δ(CH_2) band is broadened to the low-frequency side.

These features of the α-phase of OOO are similar to those of the so-called sub-α-phase,[17−23] to which the α-phase of ordinary saturated monoacid TAGs transforms reversibly by cooling. Contrary to the α-phase having the H subcell, the sub-α-phase is characterized by the p-H subcell, where hydrocarbon chains are packed in an anisotropic $O_\perp$ like subcell. Indeed, the PXD profile of OOO in Figure 3c is similar to that of SSS at 233K (Figure 5a) which can be regarded as a transition state to the sub-α-phase as described later. We found that the observed PXD profile can be decomposed into three components at 2θ = 20.5 (d = 4.33 Å), 21.5 (d = 4.13 Å), and 23.4° (d = 3.80 Å) as illustrated in Figure 3c.

On the basis of the 2θ values of the three components, the two peaks at 20.5 (d = 4.33 Å) and 23.4° (d = 3.80 Å) can be assigned to the 110 and 200 reflections of the p-H subcell, and the third component at 21.5° (d = 4.13 Å) can be assigned to the 100 reflection of the H subcell. We will discuss the issue concerning the large width of the third component in detail later. According to the above discussion, it is reasonable to

dx.doi.org/10.1021/jp4034062 | J. Phys. Chem. B 2013, 117, 8896–8905

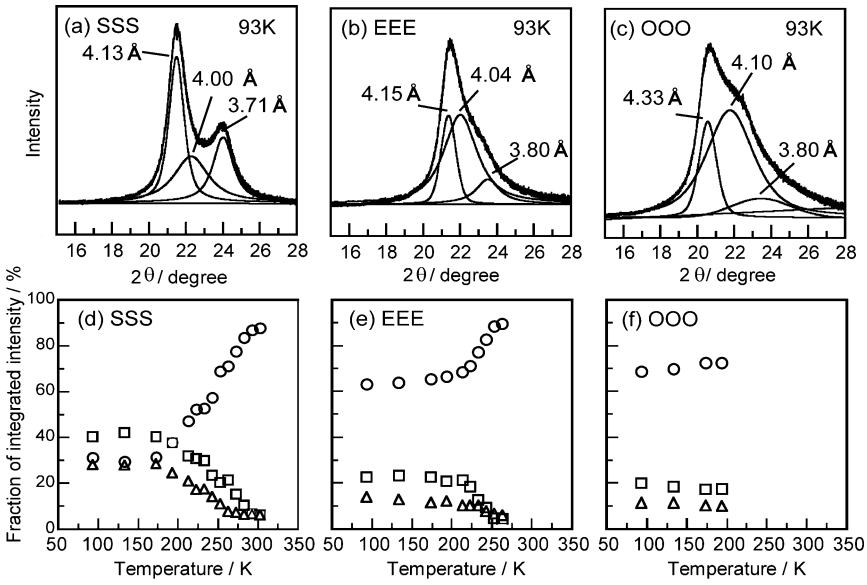

Figure 7. Analyses of PXD data of SSS, EEE, and OOO: (a–c) examples of decomposition of PXD profile into three components due to the H and p-H subcells, and (d–f) temperature dependence of intensity fractions for the three components. In (d–f), circles represent the intensity fraction of the central H-subcell reflection, and squares and triangles represent those of the 110 and 200 reflections due to the p-H subcell.

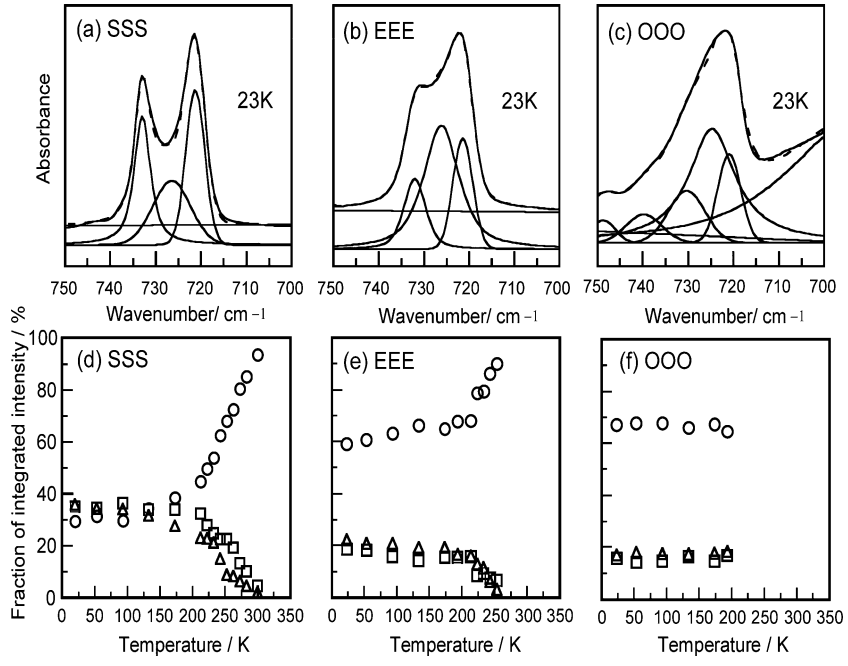

Figure 8. Analyses of infrared $r(CH_2)$ region in SSS, EEE, and OOO: (a–c) examples of decomposition of the $r(CH_2)$ band into the central component due to the H subcell and the doublet components due to the p-H subcell, and (d–f) temperature dependence of intensity fractions for the three components. In (d–f), circles represent the intensity fraction of the central component, and squares and triangles represent those of the high- and low-frequency components of the doublet.

consider that a significant proportion of acyl chains in OOO form a lateral packing similar to the p-H subcell in the α-phase, though the term "α" usually suggests the H subcell structure of acyl chains.

Structural Changes in the Course of Cooling. Figure 5 shows the changes of the PXD profile in the course of cooling for the α-phase of the three TAGs, among which SSS exhibits the most significant changes. As the temperature decreases, the reflection at 2θ = 21.4° (d = 4.15 Å) due to the H subcell becomes asymmetric and then splits into a doublet. The doublet peaks shift with temperature, and appear at 21.5° (d = 4.13 Å) and 24.0° (d = 3.71 Å) at 93 K. The temperature dependence of EEE is not so large as that of SSS. The reflection at 21.5° (d = 4.13 Å) becomes asymmetric and greatly broad but such a clear splitting does not appear. OOO exhibits quite different behavior. Although the subcell reflection is already asymmetric and broad even at a temperature near the melting point, it shows no clear change in the course of cooling.

The IR $r(CH_2)$ and $\delta(CH_2)$ regions exhibit similar tendencies as shown in Figure 6. As for SSS in Figure 6a, the $r(CH_2)$ band at 722 cm^{-1} begins to split around 243 K and clearly appears as a doublet at 733 and 721 cm^{-1} at 23 K. In

dx.doi.org/10.1021/jp4034062 | J. Phys. Chem. B 2013, 117, 8896–8905

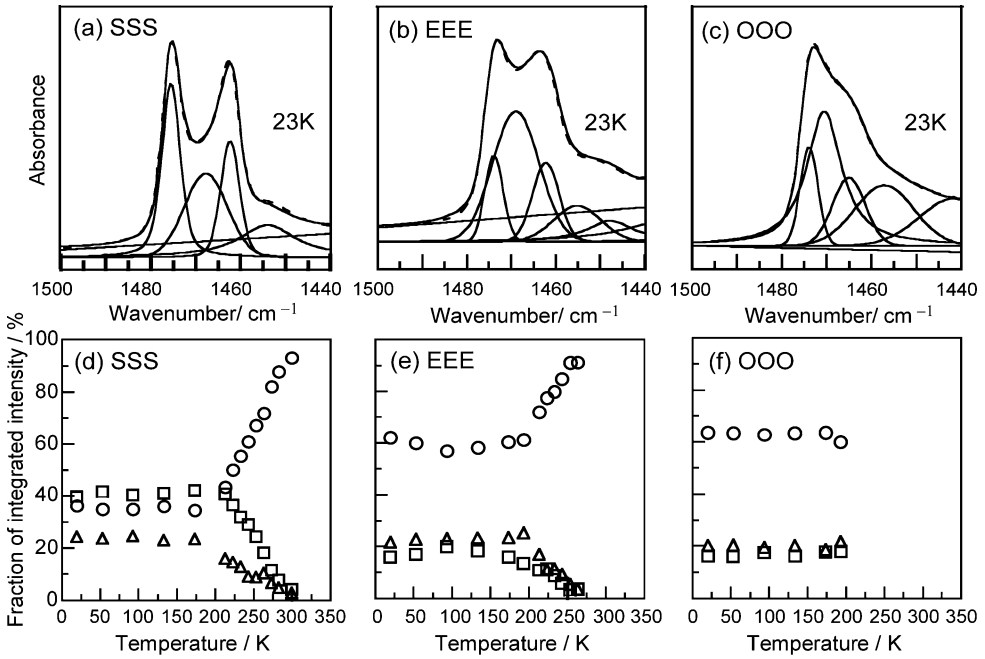

Figure 9. Analyses of infrared $\delta(CH_2)$ region in SSS, EEE, and OOO: (a–c) examples of decomposition of the $\delta(CH_2)$ band into the central component due to the H subcell and the doublet components due to the p-H subcell, and (d–f) temperature dependence of intensity fractions for the three components. In (d–f), circles represent the intensity fraction of the central component, and squares and triangles represent those of the high- and low-frequency components of the doublet.

EEE, an obvious shoulder emerges and develops around 730 cm^{-1} as shown in Figure 6b. Similarly, the $\delta(CH_2)$ band splits clearly into two bands at 1475 and 1462 cm^{-1} in SSS, and at 1473 and 1463 cm^{-1} in EEE, as shown in Figure 6, d and e. On the contrary, no such clear spectral changes take place in OOO (Figure 6c,f). Only the following small changes appear in the cooling process: the $r(CH_2)$ band becomes slightly broader on the high-frequency side, and the shoulder of the $\delta(CH_2)$ band on the low-frequency side becomes pronounced, as shown in Figure 6c,f. From these experimental results, it can be inferred that in the course of cooling the H subcell transforms to the p-H subcell mostly in SSS and partially in EEE, while no major changes take place concerning the subcell structure of OOO.

The gradual changes of PXD and IR profiles by cooling in SSS and EEE suggest that the H and p-H subcells coexist in a wide temperature range and that the ratio of the hydrocarbon chains in the H subcell to those in the p-H one successively declines as the temperature decreases. Indeed, the subcell reflection in PXD diagrams and the $r(CH_2)$ and $\delta(CH_2)$ bands in IR spectra measured at low temperatures can be decomposed into the H and p-H components, as shown in Figures 7, 8, and 9. With this two-phase model, we discuss the structural change of the three TAGs quantitatively in the next section.

Quantitative Analysis of PXD and IR Data. The complicated PXD profile observed at low temperatures for the three TAGs can be ascribed to the three reflections caused by the H and p-H subcells, as shown in Figure 7a–c. As for SSS, it can be decomposed into three reflections at 2θ = 21.5 (d = 4.13 Å), 22.2 (d = 4.00 Å), and 24.0° (d = 3.71 Å), among which the first and third are assigned to the 110 and 200 reflections of the p-H subcell and the second is assigned to the 100 reflection of the H subcell. Similarly, it can be decomposed into the three reflections at 2θ = 21.4 (d = 4.15 Å), 22.0 (d = 4.04 Å), and 23.4° (d = 3.80 Å) for EEE and at 20.5 (d = 4.33 Å), 21.7 (d = 4.10 Å), and 23.4° (d = 3.80 Å) for OOO. The intensity fractions of these three components in this region depend on temperature, as shown in Figure 7d–f. It can be regarded that the intensity fractions reveals the weight fraction of acyl chain segments in each type of subcell structure. As the temperature decreases, the fraction of the H phase decreases down to about 30% in SSS and about 60% in EEE, while it remains almost unchanged at around 70% in OOO.

Similar treatments can also be applied to the IR spectra in the $r(CH_2)$ and $\delta(CH_2)$ regions, as shown in Figures 8 and 9. The absorption in the $r(CH_2)$ region can be decomposed into three components, a central band due to the H subcell and a doublet on both sides due to the p-H subcell. For example, SSS exhibits the H component at 727 cm^{-1} and the p-H doublet at 733 and 721 cm^{-1} at 23 K, as shown in Figure 8a. Even at this very low temperature, the profile cannot be reproduced without the central H component, suggesting that the lateral packing of acyl chains does not completely transform from the H subcell to the p-H subcell. Similarly, the $r(CH_2)$ absorption mainly consists of the three components at 726 cm^{-1} (H), 732 and 721 cm^{-1} (p-H) in EEE, and 725 cm^{-1} (H), 730 and 721 cm^{-1} (p-H) in OOO, as shown in Figure 8b,c. The spectral changes in this region can be reproduced as variations in the absorption intensity fractions of the three components for all the three TAGs, as shown in Figure 8d–f. The intensity fractions of the central H band and the p-H doublet are considered to be proportional to the number of CH_2 groups in the H and p-H subcells, respectively. As observed in the PXD measurements, the H and p-H components show a decrease and an increase as the temperature decreases for SSS and EEE, while there is no clear change for OOO.

The same kind of analysis can be applied to the IR $\delta(CH_2)$ region of 1490–1450 cm^{-1} by decomposing it into three components: at 23 K the central component of the H subcell and the doublet components of the p-H subcell appear at 1468, 1476, and 1462 cm^{-1} for SSS, at 1469, 1474, and 1462 for EEE,

dx.doi.org/10.1021/jp4034062 | J. Phys. Chem. B 2013, 117, 8896–8905

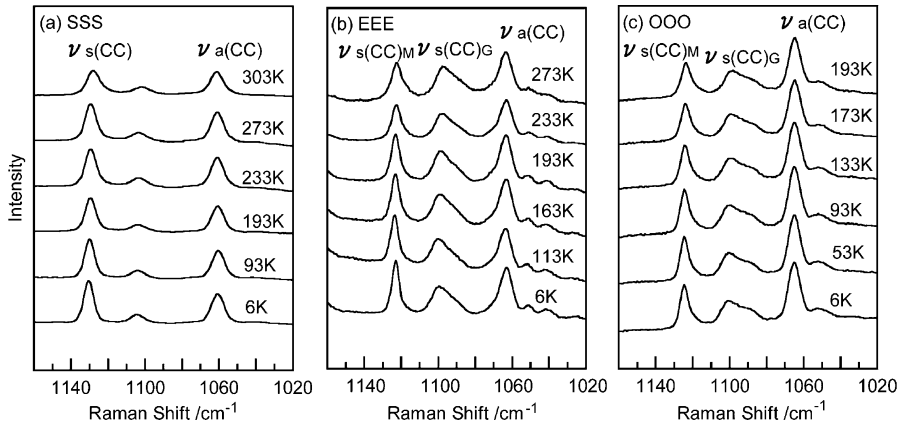

Figure 10. Temperature dependence of Raman spectra in the CC stretch region. The subscripts M and G denote the methyl side and glycerol side, respectively.

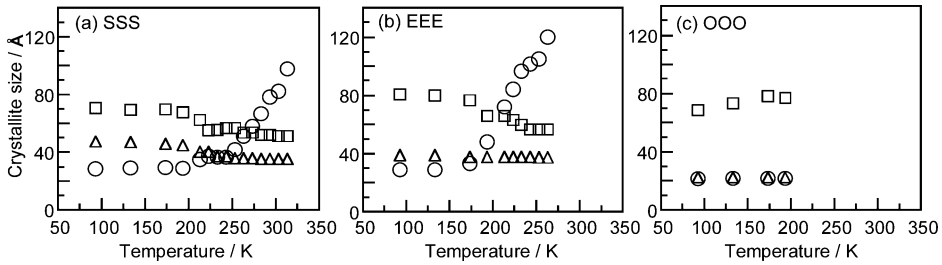

Figure 11. Temperature dependence of the H and p-H subcell domain sizes. Circles, the H domain size estimated by the 100 reflection; squares and triangles, the p-H domain sizes estimated by 110 and 200 reflections.

and at 1471, 1474, and 1465 cm^{-1} for OOO, as shown in Figure 9a–c. The intensity fractions of the three components vary almost the same way as observed in the r(CH_2) region in the course of cooling, as shown in Figure 9d–f.

As can be seen in Figures 7–9, the PXD and IR data show essentially the same results concerning the temperature dependence of the lateral packing of acyl chains. From the intensity changes of the H and p-H subcell components, the weight fraction of hydrocarbon chains stored in each subcell can be estimated, giving the following characteristics for each TAG.

The saturated TAG SSS exhibits the most pronounced subcell transformation. Although most acyl chains form the H subcell at 313 K, the fraction of the p-H subcell increases up to about 60% while the temperature decreases to about 193 K. However, further cooling hardly increases the fraction of the p-H subcell. Similarly, the H subcell prevails in EEE near the melting point, and it transforms to the p-H subcell as the temperature decreases. However, about 60% of hydrocarbon chains remain in the state of the H subcell even at the lowest temperature. On the contrary, about 40% of hydrocarbon chains in OOO form the p-H subcell even just below the melting point. The fraction of the p-H subcell hardly changes in the whole temperature range.

Spectral Change in the Raman CC Stretch Region. The Raman CC stretch region is sensitive to the conformational regularity of hydrocarbon segments. Long-chain compounds having ordered saturated hydrocarbon chains give two intense bands at about 1130 and 1060 cm^{-1} due to symmetric CC stretch ν_s(CC) and antisymmetric CC stretch ν_a(CC) modes.[24,31−33]

As for SSS, the ν_s(CC) and ν_a(CC) bands appeared at 1129 and 1060 cm^{-1} as shown in Figure 10a. As described in the previous paper,[16] OOO shows two ν_s(CC) bands at 1125 and 1095 cm^{-1}, which are respectively assigned to the methyl-sided and glycerol-sided chains, and one ν_a(CC) band at 1063 cm^{-1} due to both the methyl-sided and glycerol-sided chains. The three bands at 1125, 1095, and 1063 cm^{-1} in EEE can be assigned in the same way. The asymmetric broad band at 1095 cm^{-1} in OOO and EEE suggests a decrease in conformational regularity in the glycerol-sided chain.

In SSS the ν_s(CC) band at 1129 cm^{-1} becomes sharp as the temperature falls, which can be ascribed to a decrease in the thermal vibration of acyl chains. In EEE and OOO, there is a strong contrast between the two ν_s(CC) bands. The methyl-sided ν_s(CC) band became sharp with a decrease in temperature, whereas the glycerol-sided one remains almost unchanged, suggesting that many conformational defects persist in the glycerol-sided chain even in the low-temperature region. The sharpening of the methyl-sided ν_s(CC) band accompanied by an increase in peak height intensity is more pronounced in EEE than in OOO.

From the spectral changes above, it can be inferred that, although the conformational regularity of acyl chains tends to rise as the thermal motion freezes, the conformation disorders in the glycerol-sided chain of EEE and OOO are hardly dispelled in the process of cooling.[7,16]

Crystallite Sizes. In order to clarify how the domain of hydrocarbon chains taking the p-H subcell generates and grows on cooling, the sizes of the H and p-H subcell domains have been estimated from the 100 reflection of the H subcell and the 110 and 200 reflections of the p-H subcell by applying the Scherrer equation. Figure 11 shows the temperature dependence of the H and p-H subcell domain sizes.

As the temperature decreases from 313 to 193 K, the domain size of the H subcell decreases significantly from 100 to 30 Å

dx.doi.org/10.1021/jp4034062 | J. Phys. Chem. B 2013, 117, 8896−8905

for SSS. Similarly, it decreases from 120 to 30 Å by cooling from 273 to 173 K for EEE. However, the domain size of the H subcell hardly changes by further cooling for both SSS and EEE. The domain size of the p-H subcell increases with decreasing temperature for SSS and EEE, though there is a difference in the direction of domain growth. The p-H domain grows both in the directions perpendicular to the {110} planes and in the directions perpendicular to the {200} planes for SSS, whereas it grows solely in the direction perpendicular to the {110} planes for EEE. In both cases, the direction perpendicular to the {110} plane is the principal growth direction. As for OOO, the domain sizes of the H and p-H subcells remained almost unchanged in the process of cooling, and the H subcell domain is rather smaller in OOO than in SSS and EEE, in particular, at higher temperatures, which suggests that the large steric hindrance of the cis-olefin group would prevent the domain of the H subcell of high symmetry from growing in size.

As shown in Figure 11a,b, the domain size of the H subcell decreases close to one-third as the H to p-H subcell transformation proceeds for SSS and EEE, which suggests that a domain of the H subcell reduces in area on average by about 1 order of magnitude. On the other hand, the domain size of the p-H subcell does not increase so much. While the weight fraction of hydrocarbon segments in the p-H subcell increases about 7 times by cooling from 303 to 93 K (Figures 7–9), the domain size of the p-H subcell in the principal growth direction increases only 1.4 times for SSS. As for EEE, about a 4 times increase of the weight fraction is accompanied by a 1.3 times increase of the domain size.

Therefore, the increase in the weight fraction of the p-H subcell cannot be explained solely by the expansion of the domain in the lateral direction. One possibility to interpret the results is that, in addition to the lateral growth, an increase in the number of the domain is also contributed to the increase of the weight fraction. If multiple new domains of the p-H subcell are generated in a domain of the H subcell, the continuity of the H subcell in the domain would deteriorate, leading to a fall in the average domain size of the H subcell. Further research is needed to clarify the mechanism of the domain size change.

Effect of Trans- and Cis-Unsaturation. As described above, it has been clarified that both trans- and cis-unsaturation of acyl chains in TAGs affect significantly the lateral packing and its temperature dependence. In SSS having three saturated acyl chains, the lateral packing changes smoothly from the H subcell to the p-H subcell in the course of cooling. The weight fraction of the hydrocarbon segments taking the p-H subcell increases up to around 70% for SSS, while it increases similarly but only up to around 40% for EEE having trans-unsaturated acyl chains, OOO with three cis-unsaturated acyl chains shows the following unique characteristics, which are completely different from those of SSS and EEE.

1. About 40% of hydrocarbon chains take the p-H subcell even at temperatures close to the melting point.
2. The fraction of hydrocarbon chains having the p-H subcell does not increase in the course of cooling.
3. The cross-sectional area of the p-H subcell is significantly larger in OOO than in SSS and EEE, as shown by squares in Figure 12a.
4. Although the cross-sectional area of the H subcell increases in the order of SSS, EEE, and OOO as shown in Figure 12b, the difference is not so obvious when compared to the p-H subcell.

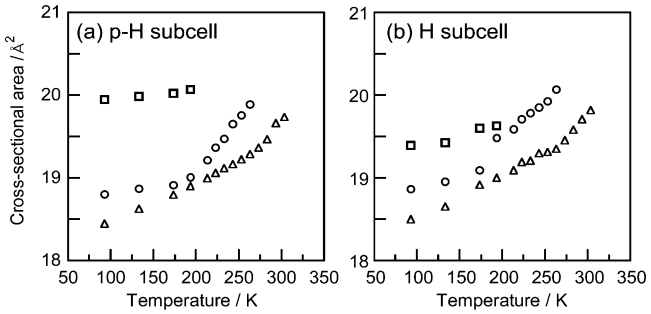

Figure 12. Temperature dependence of the cross-sectional area per chain for the p-H subcell (a) and the H subcell (b). Triangles, circles, and squares represent the cross-sectional area in SSS, EEE, and OOO, respectively.

5. The temperature dependence of the cross-sectional area is small when compared with that in SSS and EEE, in particular, for the p-H subcell.

One of the important characteristics common to SSS and EEE is that not all hydrocarbon segments change their lateral packing from the H subcell to the p-H subcell, which makes a striking contrast to *n*-alkanes and *n*-alcohols where all hydrocarbon segments participate in such structural changes.[23,34] Even in SSS, about 30% parts of hydrocarbon segments remain in the H subcell. This characteristic of SSS and EEE is probably attributable to the most sluggish part, glycerol group, which does not become completely ordered in the crystallization to the α-phase.[7] The conformational disorder remains almost unchanged in the course of cooling, thereby restricting the structural changes of acyl chains around the glycerol group. As for EEE, trans-unsaturation seems to also affect the structural changes of acyl chains.[7]

Unsaturation in EEE and OOO may have two effects. First, it divides an acyl chain into two parts, the methyl-sided and the glycerol-sided hydrocarbon segments. Second, it disturbs the formation of tight lateral packing of acyl chains and activates its mobility. As to the latter, cis-unsaturation which bends the acyl chain into a dogleg shape as shown in Figure 13c is more effective.

As can be seen from the spectral changes in the Raman CC stretch region (Figure 10), the methyl-sided and glycerol-sided chains exhibit completely different behavior in the course of cooling. The conformational disorders in the glycerol-sided

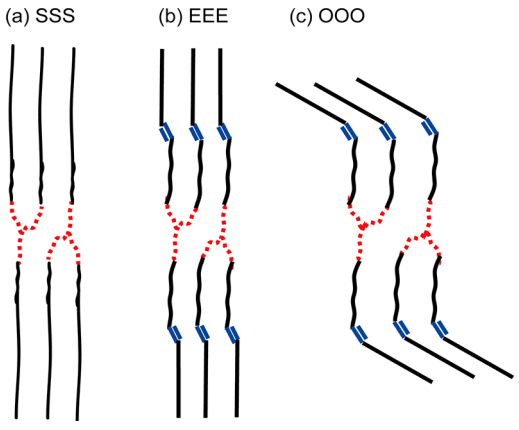

Figure 13. Molecular structure in the α-phase: (a) SSS, (b) EEE, and (c) OOO.

dx.doi.org/10.1021/jp4034062 | J. Phys. Chem. B 2013, 117, 8896–8905

chain remain almost unchanged down to 6 K, which would disturb the transformation of subcell structure. On the basis of the above discussion, we infer that the H → p-H subcell transformation in EEE takes place primarily in the methyl-sided chain.

It seems that hydrocarbon segments are hindered more effectively from forming a dense subcell structure in cis-unsaturated acyl chains of the dogleg shape than in trans-unsaturated acyl chains whose methyl-sided and glycerol-sided chains can be aligned in the same direction in solid states, as shown in Figure 13b.[6,7] We infer that this steric effect of cis-olefin group and the sluggishness of glycerol group make the glycerol-sided chains take the p-H subcell with a large cross section. If this is the case, the methyl-sided chain will incline heavily toward the lamellar surface, leading to the H subcell with a smaller cross section as shown in Figure 13c. The following two facts are consistent with this structural model. First, the conformational regularity of the glycerol-sided chain, expected to be held in the looser p-H subcell, is lower than that of the methyl-sided chains to be in the tighter H subcell. Second, the long spacing of OOO (45.2 Å) is much shorter than those of SSS (50.5 Å) and EEE (50.7 Å), which corresponds to the large inclination of the methyl-sided chain in this model.

CONCLUSION

In order to clarify the influence of cis- and trans-unsaturation on the structure and properties of the metastable α-phase of TAGs, the α-phase of three typical saturated, trans-unsaturated, and cis-unsaturated TAGs, namely, SSS, EEE, and OOO, have been investigated by means of PXD and IR and Raman spectroscopy. It is clarified that unsaturation significantly influences the lateral packing of acyl chains and its temperature dependence and that the influence appears in very different ways between cis- and trans-unsaturation. Both SSS and EEE form the H subcell in the temperature region close to the melting point, and the H subcell gradually transforms to the p-H subcell in the course of cooling. Trans-unsaturation in EEE represses the H to p-H transformation to some extent, in particular in the glycerol-sided hydrocarbon chain. On the other hand, the large steric hindrance of cis-olefin group in OOO has the effect to disturb the formation of a dense symmetric subcell structure and the contraction in the lateral direction on cooling. Even at temperature near the melting point, a fair fraction of hydrocarbon chains have the p-H subcell structure. The cross sections of the H and p-H subcells are rather larger in OOO than those in SSS and EEE and hardly change in the course of cooling.

In this study, we have studied how cis- and trans-unsaturation of acyl chains influences the structures of the two metastable α- and sub-α-phases of TAGs by using monoacid TAGs for sake of simplicity. However, most natural TAGs are mixed saturated and unsaturated fatty acid with various chain lengths, which makes the polymorphic behaviors of TAGs significantly complicated. Further studies are needed in order to elucidate the influence of unsaturation on mixed-acid TAGs.

AUTHOR INFORMATION

Corresponding Author

*Phone: +81-6-6850-5453. Fax: +81-6-6850-5288. E-mail: toshi@chem.sci.osaka-u.ac.jp.

Notes

The authors declare no competing financial interest.

REFERENCES

(1) Jensen, L. H.; Mabis, A. J. Refinement of the Structure of β-Tricaprin. *Acta Crystallogr.* **1966**, *21*, 770−781.
(2) Larsson, K. The Crystal Structure of the β-form of Trilaurin. *Ark. Kemi* **1964**, *23*, 1−15.
(3) Larsson, K. The Crystal Structure of the β-form of Triglycerides. *Proc. Chem. Soc.* **1963**, 87−88.
(4) Mykhaylyk, O. O.; Hamley, I. W. The Packing of Triacylglycerols from SAXS Measurements: Application to the Structure of 1,3-Distearoyl-2-oleoyl-*sn*-glycerol Crystal Phases. *J. Phys. Chem. B* **2004**, *108*, 8069−8083.
(5) Langevelde, A. V.; Malssen, K. V.; Hollander, F.; Peschar, R.; Schenk, H. Structure of Mono-Acid Even-numbered β-Triacylglycerols. *Acta Crystallogr.* **1999**, *B55*, 114−122.
(6) Culot, C.; Norberg, B.; Evrand, G.; Durant, F. Molecular Analysis of the Beta-Polymorphic Form of Trielaidin: Crystal Structure at Low Temperature. *Acta Crystallogr.* **2002**, *B56*, 317−321.
(7) Dohi, K.; Kaneko, F.; Kawaguchi, T. X-ray and Vibrational Spectroscopic Study on Polymorphism of Trielaidin. *J. Cryst. Growth* **2002**, *237−239*, 2227−2232.
(8) Langevelde, A. V.; Malssen, K. V.; Driessen, R.; Goubitz, K.; Hollander, F.; Peschar, R.; Zwart, P.; Schenk, H. Structure of $C_nC_{n+2}C_n$-type (n = even) β'-Triacylglycerols. *Acta Crystallogr.* **2000**, *B56*, 1103−1111.
(9) Sato, K.; Goto, M.; Yano, J.; Kodali, D. R.; Small, D. M. Atomic Resolution Structure Analysis of β' Polymorph Crystal of a Triacylglycerol: 1,2-Dipalmitoyl-3-Myristoyl-*sn*-Glycerol. *J. Lipid Res.* **2001**, *42*, 338−345.
(10) Mechelen, J. B. van; Peschar, R.; Schenk, H. Z. Structure and Polymorphism of Trans Mono-Unsaturated Triacylglycerols. *Kristallogr. Suppl.* **2009**, *30*, 491−495.
(11) Berger, K. G.; White, G. H. The Fat Globule Membrane in Ice Cream. *Dairy Ind. Int.* **1976**, *41*, 199−243.
(12) Garti, N.; Sato, K. *Crystallization Processes in Fats and Lipid Systems*; Marcel Dekker: New York, 2001.
(13) Kikukawa, K. *The Handbook of Oil Chemistry, 4th ed.; Lipids and Surfactants*; Maruzen: Tokyo, 2001.
(14) DeMan, L.; DeMan, J. M.; Blackman, B. Physical and Textural Evaluation of some Shortenings and Margarines. *J. Am. Oil Chem. Soc.* **1989**, *66*, 128−132.
(15) Rivarola, G.; Segura, J. A.; Anon, M. C.; Calvelo, A. Crystallization of Hydrogenated Sunflower-Cottonseed Oil. *J. Am. Oil Chem. Soc.* **1987**, *64*, 1537−1543.
(16) Akita, C.; Kawaguch, T.; Kaneko, F. Structural Study on Polymorphism of Cis-Unsaturated Triacylglycerol: Triolein. *J. Phys. Chem. B* **2006**, *110*, 4346−4353.
(17) Jackson, F. L.; Lutton, E. S. The Polymorphism of Certain Behenyl Mixed Triglycerides. A New Metastable Crystalline Form of Triglycerides. *J. Am. Chem. Soc.* **1950**, *72*, 4519−4521.
(18) Goto, M.; Asada, E. X-ray Diffraction of the Binary System Tristearin-Tripalmitin. *Yukagaku* **1967**, *16*, 402−406.
(19) Chapman, D. Infrared Spectroscopic Characterization of Glycerides. *J. Am. Oil Chem. Soc.* **1960**, *37*, 73−77.
(20) Kodal,i, D. R.; Fahey, D. A.; Small, D. M. Structure and Polymorphism of Saturated Monoacid 1,2-Diacyl-sn-Glycerols. *Biochemistry* **1990**, *29*, 10771−10779.
(21) Di, L.; Small, D. M. Physical Behavior of the Hydrophobic Core of Membranes: Properties of 1-Stearoyl-2-Linoleoyl-sn-Glycerol. *Biochemistry* **1995**, *34*, 16672−16677.
(22) Lutton, E. S. *Review* of the Polymorphism of Saturated Even Glycerides. *J. Am. Chem. Soc.* **1950**, *27*, 276−281.
(23) Small, D. M. *The Physical Chemistry of Lipids*; Plenum Press: New York, 1986; p 32.
(24) Garti, N.; Sato, K. *Crsytallization and Polymorphism of Fats and Fatty Acids*; Marcel Dekker: New York, 1988.

(25) Strobl, G. R.; Hagedorn, W. Raman Spectroscopic Method for Determining the Crystallinity of Polyethylene. *J. Polym. Sci. Polym. Phys.* **1978**, *16*, 1181−1193.
(26) Hindeleh, A. M.; Johnson, D. J. Crystallinity and Crystallite Size Measurement in Cellulose Fibres: 2. Viscose rayon. *Polymer* **1974**, *15*, 697−705.
(27) Jones, F. W. The Measurement of Particle Size by the X-ray Method. *Proc. R. Soc.* **1938**, *A116*, 16−43.
(28) Scherrer, P. Bestimmung der Größe und der inneren Struktur von Kolloidteilchen mittels Röntgenstrahlen. *Nachr. Ges. Wiss. Göttingen* **1918**, *26*, 98−100.
(29) Stokes, A. R.; Willson, A. J. C. A Method of Calculating the Integral Breadths of Debye-Scherrer Lines. *Proc. Cambridge Philos. Soc.* **1942**, *38*, 313−322.
(30) Warren. B. E. *X-ray Diffraction*; Dover: New York, 1990.
(31) Piseri, L.; Zerbi, G. Dispersion Curves and Frequency Distribution of Polymers: Single Chain Model. *J. Chem. Phys.* **1968**, *48*, 3561−3572.
(32) Zerbi, G.; Conti, G.; Minoni, G. Premelting Phenomena in Fatty Acids: An Infrared and Raman Study. *J. Phys. Chem.* **1987**, *91*, 2386−2393.
(33) Kobayashi, M.; Koneko, F.; Sato, K.; Suzuki, M. Vibrational Spectroscopic Study on Polymorphism and Order-Disorder Phase Transition in Oleic Acid. *J. Phys. Chem.* **1986**, *90*, 6371−6378.
(34) Dorset, D. L. *Crystallography of the Polymethylene Chain*; Oxford University Press: New York, 2005.